

# MindShot: Brain Decoding Framework Using Only One Image

Shuai Jiang<sup>1</sup>, Zhu Meng<sup>1</sup>, Delong Liu<sup>1</sup>, Haiwen Li<sup>1</sup>, Fei Su<sup>1,2</sup> and Zhicheng Zhao<sup>1,2,†</sup>

<sup>1</sup>Beijing University of Posts and Telecommunications

<sup>2</sup>Beijing Key Laboratory of Network System and Network Culture

## Abstract

Brain decoding, which aims at reconstructing visual stimuli from brain signals, primarily utilizing functional magnetic resonance imaging (fMRI), has recently made positive progress. However, it is impeded by significant challenges such as the difficulty of acquiring fMRI-image pairs and the variability of individuals, etc. Most methods have to adopt the per-subject-per-model paradigm, greatly limiting their applications. To alleviate this problem, we introduce a new and meaningful task, few-shot brain decoding, while it will face two inherent difficulties: 1) the scarcity of fMRI-image pairs and the noisy signals can easily lead to overfitting; 2) the inadequate guidance complicates the training of a robust encoder. Therefore, a novel framework named MindShot, is proposed to achieve effective few-shot brain decoding by leveraging cross-subject prior knowledge. Firstly, inspired by the hemodynamic response function (HRF), the HRF adapter is applied to eliminate unexplainable cognitive differences between subjects with small trainable parameters. Secondly, a Fourier-based cross-subject supervision method is presented to extract additional high-level and low-level biological guidance information from signals of other subjects. Under the MindShot, new subjects and pretrained individuals only need to view images of the same semantic class, significantly expanding the model's applicability. Experimental results demonstrate MindShot's ability of reconstructing semantically faithful images in few-shot scenarios and outperforms methods based on the per-subject-per-model paradigm. The promising results of the proposed method not only validate the feasibility of few-shot brain decoding but also provide the possibility for the learning of large models under the condition of reducing data dependence.

## 1 Introduction

The brain, as the core of human cognition and perception of the world, plays a pivotal role in encoding perceptual stimuli, processing them, and influencing decisions. A deeper understanding of the brain's working mechanisms requires exploring the reverse process - brain decoding. It involves the interpretation of responses from external visual stimuli to the visual cortex and reconstructing images from brain activity based on functional magnetic resonance imaging (fMRI) has become a feasible solution. Brain decoding not only reveals the brain's intricate cognitive processes [1, 2, 3], but also advances the field of brain-computer interfaces (BCI) [4, 5].

Encouraging progress has been made in brain decoding, as evolving from generative adversarial networks (GANs) [6, 7, 8, 9] to diffusion models (DMs) [10, 11, 12, 13, 14, 15] are employed for visual reconstruction, where more realistic and semantically faithful images have been generated. However, brain decoding is still facing many challenges.

Specifically, due to the lack of fMRI-image pairs and individual variability in brain representations, following a per-subject-per-model paradigm, the existing decoding frameworks [7, 8, 9, 11, 12, 13, 14, 16] are all tailored individually for each subject. In this paradigm, a decoding model first needs to be trained on a specific subject before it can be tested. When applied to new subjects, the need for rescanning the subjects’ brain activity makes the process costly and time-consuming, thereby limiting its applicability, which drives us to propose a new task: **few-shot brain decoding**, aiming to achieve visual reconstruction by training on only a few amount of fMRI-image pairs for new subjects. This design is clearly more in line with real-world scenarios than existing paradigm.

However, to achieve this goal, two challenges need to be well addressed: **1) Overfitting**: small-scale training samples can easily lead to overfitting, but this is prominent in brain decoding. **2) Lack of useful biological guidance**: the insufficient biological signals for guidance makes it difficult to efficiently train a robust brain cognition encoder in few-shot scenarios.

To address aforementioned challenges, MindShot, a Fourier-based cross-subject supervision framework is proposed to achieve few-shot brain decoding. MindShot adopts a pretrain-finetune two-stage framework. First, to learn prior knowledge on multiple subjects, a contrastive learning approach is employed, and then, the brain decoding model is finetuned using only few-shot fMRI-image pairs on new individuals. Specifically, MindShot integrates novel strategies to solve each challenge: **1) HRF adapter**: inspired by the hemodynamic response function (HRF) [17], a subject-specific adapter is designed to mimic the variability between individuals. Only the HRF adapter is trainable during the finetune phase, which effectively reduces the training cost and overfitting; **2) Fourier-based cross-subject supervision**: considering that the biological signals of other subjects are adopted as a guide, thus we use Fourier transform [18] to extract both high-level and low-level features of biological signals to effectively supervise the visual decoding of new subjects.

To validate our model, extensive experiments are conducted on the Natural Scenes Dataset (NSD) [19]. Although it is the largest dataset in the field of brain visual decoding, the maximum number of shared images viewed by all subjects is only 1000, highlighting the few-shot learning difficulty. Therefore, MindShot introduces a comprehensive cross-subject supervision approach, in which new and pretrained subjects only need to view images in the same semantic class, thus expanding the model’s applicability. Additionally, MindShot can synthesize images with semantic fidelity by simply training a few parameters, significantly outperforming the state-of-the-art (SOTA) methods based on per-subject-per-model paradigm.

Our contributions are summarized as follows:

- A new few-shot brain decoding task is designed and a few-shot brain decoding framework - MindShot is accordingly proposed to alleviate the scarcity of new individual fMRI-image pairs by introducing cross-individual prior.
- A lightweight HRF adapter with Fourier-based cross-subject supervision is constructed to eliminate inter-individual differences and synthesize images with semantic fidelity.
- Extensive experiments demonstrate the effectiveness and practicality of MindShot, and the results show that the MindShot outperforms the SOTA methods under per-subject-per-model paradigm.

## 2 Related work

### 2.1 Brain decoding

The development of brain decoding is closely related to the evolution of decoding methods for brain activity. In early years, Horikawa *et al.* [4] found that different layers of image representations from deep neural networks (DNNs) correlate with neural activity in the visual cortex of the human brain. Inspired by this finding, Shen *et al.* [20] designed the feature decoder to map fMRI patterns to multi-layer pretrained DNN features of real images. With the advent of Generative Adversarial Networks (GANs) [6], researchers had shifted fMRI modalities from mapping to DNNs to the latent space of GANs, which facilitated the reconstructing of human faces [21, 22, 23] and natural images [7, 8, 9].

Recently, the framework of brain decoding has been greatly advanced by the breakthrough of multimodal technologies, especially contrastive learning [24, 25] and Diffusion models (DMs)

[10, 26]. Researchers worked to map fMRI data to a variety of supervised information, including high-level CLIP semantic embedding [11, 12, 13, 14, 15], and low-level depth [27] and color [28] features. Then, the encoded brain activity was fed to DMs, synthesizing high-quality images with semantic fidelity and sufficient detail. Most recently, Wang *et al.* [29] has achieved cross-subject brain decoding with a single model using a cyclic fMRI reconstruction mechanism. Unlike most brain decoding research, which typically requires numerous fMRI-image pairs to train models, MindShot focuses on new subject brain decoding with only few-shot samples.

## 2.2 Diffusion probabilistic models

DMs showed unlimited potential in multiple applications [30, 31, 32, 33, 34, 35, 36], related to multimodal and generative artificial intelligence. DMs leveraged prior knowledge from large-scale image-text pairs [37] and demonstrated remarkable ability in synthesizing high-quality images characterized by high semantic fidelity and resolution. To reduce the computational cost, Rombach *et al.* [26] employed a variational auto-encoder (VAE) to transfer the denoising process to the latent space. ControlNet [38] and IP-Adapter [39] aimed to enhance the control of the image generation process by fusing other information such as sketch, depth, and spatial palette. Versatile Diffusion (VD) [40] facilitated the utilization of multimodal capabilities and demonstrated effectiveness in brain decoding studies. Leveraging the powerful generative model of VD and inspired by [29] on cross-subject brain decoding, a Fourier-based cross-subject supervision approach is proposed to alleviate the scarcity of new individuals in real-world application scenarios.

## 3 Methodology

### 3.1 Issue definition: few-shot brain decoding task

In few-shot brain decoding tasks, images are classified into 80 semantic classes based on the NSD dataset’s image labels. Within each semantic class, a few images are randomly selected as visual stimuli to simulate real-world data deficiency scenarios. Based on the above few-shot settings, this task will explore whether brain decoding can still be effectively implemented.

### 3.2 MindShot

In response to aforementioned question, MindShot, a Fourier-based cross-subject supervision framework is proposed to achieve few-shot brain decoding. As shown in 1, MindShot employs a two-stage network. Firstly, it uses contrastive learning to acquire prior knowledge from multiple subjects. Then, the brain decoding model is finetuned using only a few-shot fMRI-image pairs.

**Prior knowledge pretrain.** Current brain decoding frameworks [7, 11, 14, 12] develop subject-specific brain decoders by mining the statistical distribution of subjects through large fMRI-image pairs. However, in few-shot settings, this approach becomes ineffective due to the scarcity of data. Previous work [16] employed Masked Image Modeling (MIM) [41] for pretraining, where a substantial amount of fMRI signals unrelated to visual stimuli was employed, thereby lacking explicit semantic supervision. In contrast, a contrastive learning approach is employed to obtain prior knowledge with high semantic alignment. Specifically, as illustrated in Figure 1 (b), multiple subjects are utilized to pretrain the visual decoding model  $\mathcal{M}$ , with their fMRI voxels denoted as  $x_1, \dots, x_j$ , where  $x \in \mathbb{R}^{1 \times N}$ , and the corresponding visual stimuli as  $I_1, \dots, I_j$ , where  $I \in \mathbb{R}^{H \times W \times 3}$ . Only the brain encoder  $\mathcal{E}_{brain}$  is trained using the contrastive learning method, employing the loss function  $\mathcal{L}_c$  [12], thereby equipping the model  $\mathcal{M}$  with prior knowledge from multiple subjects. This structure allows for learning common semantic features and representations across multiple subjects, enhancing transferability on new subjects. In addition, the flexible framework allows for pretraining on larger datasets and more diverse subjects, acquiring richer prior knowledge.

**New subject few-shot adaptation.** With the prior knowledge obtained from multiple subjects’ brain decoding, the straightforward approach is to utilize the pretrained weights of the parameters and finetuning with all layers open. However, due to the limited shared images among different subjects in the NSD dataset, this approach lacks clear guidance to fully utilize prior knowledge, especially considering significant individual differences. Signals’ frequency domain holds high-level semantics

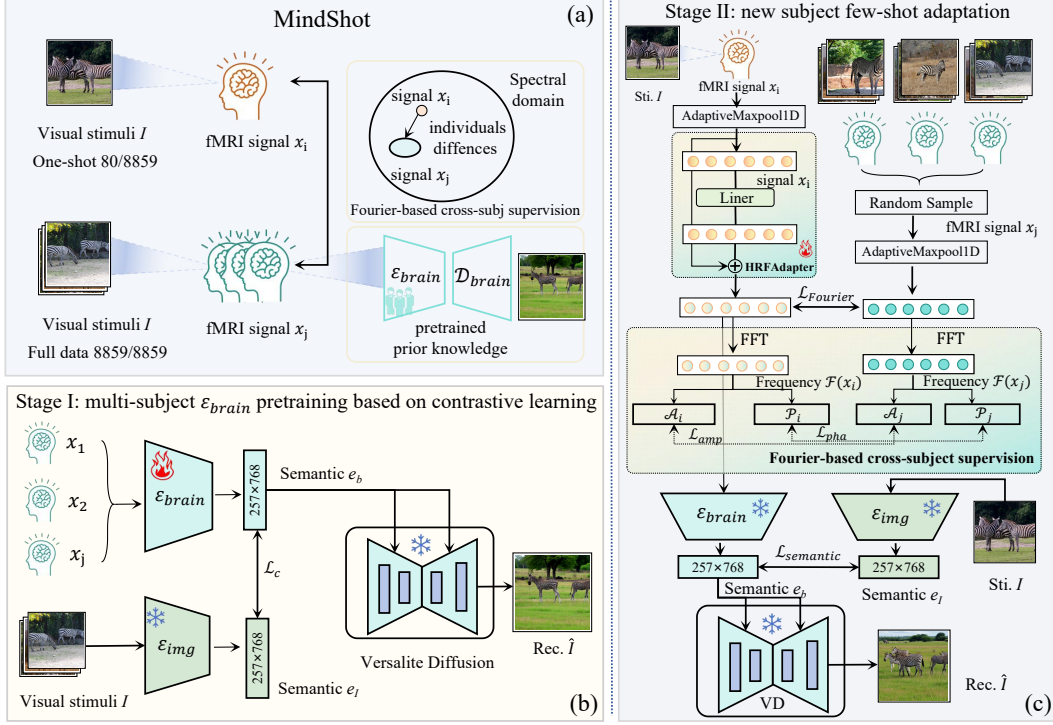


Figure 1: The overall architecture of MindShot. (a) MindShot is a Fourier-based cross-subject framework capable of achieving few-shot brain decoding. (b) The contrastive learning approach is utilized to acquire prior knowledge. (c) The hemodynamic response function (HRF) adapter is trained via Fourier-based cross-subject supervision to facilitate adaptation in new subjects with few-shot fMRI-image pairs. The semantic embeddings are then fed into versatile diffusion model for image reconstruction.

and low-level statistical information, offering richer information than raw signals. Therefore, the proposed HRF adapter equipped with Fourier-based cross-subject supervision aims to eliminate individual differences and maximize prior knowledge utilization. Specifically, as shown in Figure 1 (c), the fMRI voxels  $x_i$  of new subjects are scaled to a uniform scale using an adaptive maxpooling layer. Subsequently, an individual HRF adapter, systematically modeled after the hemodynamic response, is applied to correct biases between subjects, resulting in voxel  $\hat{x}_i$ . Meanwhile, samples are randomly selected from the pretrained subjects, and their corresponding fMRI voxels  $x_j$  are also downsampled to a uniform scale. Then, their voxels  $\hat{x}_i$  and  $\hat{x}_j$  are transformed into the spectral domain using FFT [18] to obtain  $\mathcal{F}(x_i)$  and  $\mathcal{F}(x_j)$ , respectively. Then, the corresponding amplitudes and phases  $\mathcal{A}_i, \mathcal{A}_j, \mathcal{P}_i, \mathcal{P}_j$  are calculated separately to achieve cross-subject supervision. Once training,  $\hat{x}_i$  is fed into the pretrained brain encoder  $\mathcal{E}_{brain}$ , which has acquired prior knowledge from multiple individuals, to generate the semantic embedding  $e_{brain}$ . Then, the embedding is used as a control condition to guide the brain decoder  $\mathcal{D}_{brain}$  to produce the reconstructed image  $\hat{I}$ .

### 3.3 HRF adapter

Existing experiment has shown that regions of interest (ROIs) in the visual cortex vary in location and size from one individual to another for the same visual stimulus, which leads to large differences in voxels between individuals [16]. To eliminate such differences, inspiration is drawn from the hemodynamic response function (HRF) [17, 15], and the HRF adapter is designed according to its theoretical modeling.

The HRF is typically used to model the relationship between neural activity and the Blood Oxygenation Level Dependent (BOLD) signal. In a linear time-invariant (LTI) system, the signal  $y(t)$  at time  $t$  is considered as the convolution of the stimulus function  $s(t)$  and the hemodynamic response  $h(t)$ , denoted as  $y(t) = (s * h)(t)$ . The  $h(t)$  is usually modeled as a linear combination of basis functions

that can be integrated into a matrix form:  $\mathbf{Y} = \mathbf{X}\beta + \mathbf{e}$ , where  $\mathbf{Y}$  denotes the observed fMRI voxels,  $\beta$  is a vector of regression coefficients, and  $\mathbf{e}$  is a vector of unexplained error values.

However,  $\mathbf{e}$  varies significantly among individuals and sessions due to factors like age and cognitive state, which affect firing rate, onset latency, and neuronal activity duration. These variations influence the estimation of  $\mathbf{e}$  and ultimately impact the accuracy of fMRI-based brain decoding.

In the new subject few-shot adaptation phase, let  $X_i$  and  $X_j$  represent the visual stimuli for two different subjects. The matrices of hemodynamic response for two subjects are given by  $\mathbf{Y}_i = \mathbf{X}_i\beta + \mathbf{e}_i$  and  $\mathbf{Y}_j = \mathbf{X}_j\beta + \mathbf{e}_j$ . The difference error  $\mathbf{e}_d$  between individuals is defined as  $\mathbf{e}_d = |\mathbf{e}_j - \mathbf{e}_i|$ . The hemodynamic response matrix for the new subject after compensation can be represented as:

$$\hat{\mathbf{Y}}_i = \mathbf{X}_i\beta + \mathbf{e}_i + \mathbf{e}_d. \quad (1)$$

Thus, from the signal processing perspective, only a mapping function  $f(x)$  corresponding to the difference error  $\mathbf{e}_d$  needs to be learned. The HRF adapter adopts a residual structure, and the output is formulated as:

$$\hat{x}_i = x_i + f(x_i), \quad (2)$$

where  $f(\cdot)$  is implemented using a linear layer. By applying the HRF adapter, neural response patterns between subjects can be aligned, thereby reducing inter-subject variability in fMRI data. Additionally, the HRF adapter provides a learnable data augmentation method by accounting for individual variations in the hemodynamic response function, contributing to more accurate and reliable brain decoding results.

### 3.4 Fourier-based cross-subject supervision

Our motivation comes from the previous findings of Fourier transformation that the phase component of Fourier spectrum preserves high-level semantics of the original signal, while the amplitude component contains low-level statistical information, which is generally regarded as style information [42, 43, 44, 45, 46]. For a subject's brain signal  $x$ , its Fourier transformation is formulated as:

$$\mathcal{F}(x) = \sum_{n=0}^{N-1} x(k) e^{-j2\pi \frac{nk}{N}}, k = 0, 1, \dots, K-1, \quad (3)$$

where  $K$  represents the length of Fourier spectrum signal. The Fourier transformation can be calculated with the FFT algorithm [18] efficiently. The amplitude and phase components are then respectively represented as:

$$\mathcal{A}(x) = [R^2(x) + I^2(x)]^{\frac{1}{2}}, \mathcal{P}(x) = \arctan\left[\frac{I(x)}{R(x)}\right], \quad (4)$$

where  $R(x)$  and  $I(x)$  represent the real and imaginary part of  $\mathcal{F}(x)$ , respectively. For new and pretrained subjects, brain voxels  $x_i$  and  $x_j$  are downsampled and transformed by the HRF adapter to obtain signals  $\hat{x}_i$  and  $\hat{x}_j$ . Subsequently, the corresponding amplitudes and phases of Fourier spectrum,  $\mathcal{A}_i, \mathcal{A}_j, \mathcal{P}_i, \mathcal{P}_j$ , are calculated separately. Then, the losses for  $\mathcal{L}_{amp}$  and  $\mathcal{L}_{pha}$  are computed as follows:

$$\mathcal{L}_{amp} = \frac{1}{N} \sum_{n=0}^{N-1} (\mathcal{A}_i - \mathcal{A}_j)^2, \mathcal{L}_{pha} = \frac{1}{N} \sum_{n=0}^{N-1} (\mathcal{P}_i - \mathcal{P}_j)^2. \quad (5)$$

The Fourier loss integrates both the high-level semantics and low-level statistical information of the original signal. Its expression is as follows:

$$\mathcal{L}_{Fourier} = \mathcal{L}_{amp} + \mathcal{L}_{pha}. \quad (6)$$

To ensure the semantic fidelity of brain visual reconstruction for new individuals, the SoftCLIP loss [12] and prior loss [47] are utilized, which has proven effective in aligning the fMRI modality with the CLIP embedding space. The SoftCLIP loss is defined as:

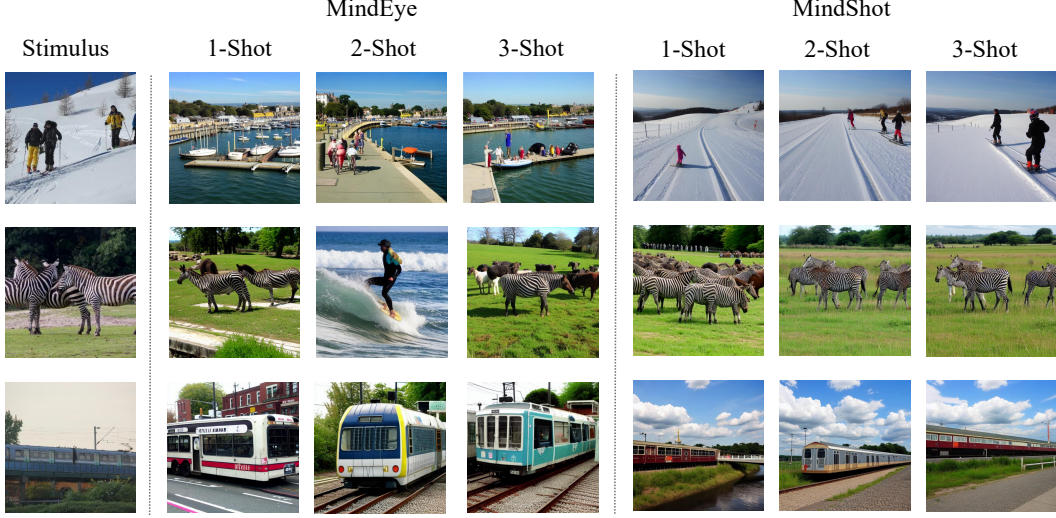


Figure 2: Visualization of few-shot brain decoding. The per-subject-per-model represented by MindEye suffers from serious semantic errors with few samples, e.g., skiing is misinterpreted as a lake. In contrast, our proposed MindShot, a Fourier-based cross-subject supervision framework, excels at reconstructing images in few-shot scenarios.

$$\mathcal{L}_{SoftCLIP}(e_b, e_I) = - \sum_{i=0}^{N-1} \sum_{j=0}^{N-1} \left[ \frac{\exp(e_i^I \cdot e_j^I / \tau)}{\sum_{m=0}^{N-1} \exp(e_i^I \cdot e_m^I / \tau)} \cdot \log \left( \frac{\exp(e_i^b \cdot e_j^I / \tau)}{\sum_{m=0}^{N-1} \exp(e_i^b \cdot e_m^I / \tau)} \right) \right], \quad (7)$$

where  $e_b$  and  $e_I$  are the semantic embeddings of brain and visual stimuli in a batch of size  $B$ , respectively, and  $\tau$  is a temperature hyperparameter. The semantic loss is defined as:

$$\mathcal{L}_{semantic} = \mathcal{L}_{softCLIP} + \mathcal{L}_{prior} \quad (8)$$

Therefore, in the new subject few-shot task, the HRF adapter is trained end-to-end using  $\mathcal{L}_{total}$  to achieve brain activity visual reconstruction.

$$\mathcal{L}_{total} = \mathcal{L}_{semantic} + \mathcal{L}_{Fourier} \quad (9)$$

## 4 Experiments

### 4.1 Implementation details

**Dataset.** The Natural Scenes Dataset(NSD) [19] is employed to evaluate the effectiveness of MindShot. NSD, as the largest dataset in the field of brain activity visual reconstruction, comprises high-resolution 7 Tesla fMRI scans obtained from 8 healthy subjects. These subjects are instructed to observe a total of 73,000 natural images from the MS-COCO dataset [48], which are categorized into 80 semantic classes based on their captions. The training set of each subject involved 8,859 images, while the test set consisted of 982 images. Only 1,000 images are viewed by all 8 subjects, with 982 of these included in the testing set; the remaining 18 images are negligible. Following other brain decoding studies [11, 49, 12, 29], our research focused on four subjects who completed all scanning sessions (subjects 1, 2, 5, and 7).

**Evaluation metrics.** To evaluate the effectiveness of our approach, several metrics used to assess the quality of image reconstruction are employed. These include low-level metrics such as PixCorr, SSIM [50], AlexNet(2), and AlexNet(5) [51], and high-level metrics such as Inception [52], CLIP [25], EffNet-B [53], and SwAV [54].





Figure 3: Results of the one-shot brain decoding for subject 1, 2, 5, and 7.

Table 1: Results of few-shot brain decoding. All metrics are calculated as the average across 4 subjects. The NSD dataset comprises 80 semantic classes of visual stimuli, from which 1 to 3 images per class are randomly sampled to form a subset. To ensure a fair comparison, MindEye [12] employs the same experimental settings and leverages prior knowledge from other subjects. Additionally, an adaptive max pooling layer is incorporated for fMRI signal scale normalization [29]. MindShot significantly outperformed the per-subject-per-model paradigm in all few-shot scenarios.

| Method         | Data   | Low-Level   |             |              |              | High-Level   |              |             |             |
|----------------|--------|-------------|-------------|--------------|--------------|--------------|--------------|-------------|-------------|
|                |        | PixCorr↑    | SSIM↑       | Alex(2)↑     | Alex(5)↑     | Incep↑       | CLIP↑        | Eff↓        | SwAV↓       |
| MindEye        | 1-shot | .047        | .213        | 62.3%        | 68.9%        | 61.5%        | 66.4%        | .927        | .601        |
| MindShot(Ours) | 1-shot | <b>.097</b> | <b>.260</b> | <b>73.8%</b> | <b>81.9%</b> | <b>73.7%</b> | <b>77.1%</b> | <b>.853</b> | <b>.533</b> |
| MindEye        | 2-shot | .069        | .237        | 68.5%        | 75.8%        | 67.5%        | 72.1%        | .896        | .574        |
| MindShot(Ours) | 2-shot | <b>.117</b> | <b>.262</b> | <b>76.9%</b> | <b>85.9%</b> | <b>78.8%</b> | <b>81.5%</b> | <b>.816</b> | <b>.499</b> |
| MindEye        | 3-shot | .079        | .249        | 71.1%        | 78.9%        | 70.2%        | 75.0%        | .879        | .555        |
| MindShot(Ours) | 3-shot | <b>.122</b> | <b>.267</b> | <b>78.8%</b> | <b>87.9%</b> | <b>81.6%</b> | <b>83.5%</b> | <b>.794</b> | <b>.482</b> |

## 4.2 Few-shot brain decoding

To validate the effectiveness of MindShot, a comparison is made with a per-subject-per-model framework using identical experimental settings. As illustrated in Table 1 and Figure 2, MindEye performs poorly on new subjects in few-shot brain decoding tasks, with the high-level metric of CLIP only 66.4%. In contrast, MindShot performs well and outperforms MindEye by nearly 11 points. Notably, in the 1-shot scenario, our method even surpasses MindEye’s performance achieved with 3-shot finetuned data. This disparity can be attributed to the per-subject-per-model

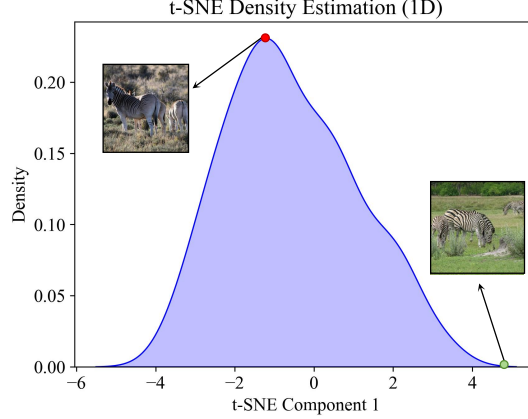


Figure 4: Visualization of one-shot selection. Taking the zebra semantic class as an example, the red and green color dots represent the visual stimulus with the highest and lowest probability density, respectively.

Table 2: Results of one-shot visual stimuli selection. The impact of three visual stimulus sampling strategies on the model training results. Kda-min and Kda-max, represent the minimum and maximum data points selected based on Gaussian probability density modeling of the subject’s fMRI data, respectively. Random denotes random sampling.

| Sample method | Data   | Low-Level   |             |              |              | High-Level   |              |             |             |
|---------------|--------|-------------|-------------|--------------|--------------|--------------|--------------|-------------|-------------|
|               |        | PixCorr↑    | SSIM↑       | Alex(2)↑     | Alex(5)↑     | Incep↑       | CLIP↑        | Eff↓        | SwAV↓       |
| Kda-min       | 1-shot | .069        | .265        | 71.4%        | 80.4%        | 71.1%        | 74.7%        | .870        | .548        |
| Random        | 1-shot | .091        | <b>.275</b> | <b>74.1%</b> | 81.8%        | 72.1%        | 75.6%        | .865        | .541        |
| Kda-max       | 1-shot | <b>.115</b> | .263        | 73.7%        | <b>82.6%</b> | <b>73.8%</b> | <b>76.7%</b> | <b>.854</b> | <b>.530</b> |

framework’s necessity to train a large number of parameters, making it prone to overfitting and lacking generalization ability for new subjects in small-sample scenarios. Conversely, MindShot employs a Fourier-based cross-subject supervision method to train lightweight HRF adapter, effectively modeling inter-individual differences and leveraging prior knowledge. Consequently, MindShot can achieve the promising visual reconstruction in few-shot scenarios. Please refer to Appendix A.6 for detailed few-shot brain decoding results for subjects 1, 2, 5, and 7.

### 4.3 One-shot visual stimuli selection

The results presented in Figure 2, 3, and Table 1 demonstrate MindShot’s capability to achieve one-shot brain decoding for multiple subjects, generating high-resolution and semantically faithful images. However, an urgent question arises: for each semantic category, which image should serve as the visual stimulus to represent the distribution of the new individual? To evaluate the impact of different visual stimuli on the outcomes, an analysis is conducted on the statistical distribution of each semantic category. As shown in Figure 4, the fMRI voxels of new subjects are categorized based on semantic categories, and the fMRI voxels for each category are reduced to 1 dimension using the t-SNE method [55]. Based on their linear distribution in the feature space, these dimensions are then modeled using a Gaussian distribution to estimate the probability density function, thus capturing the statistical distribution of the individual within each category. Three sets of experiments are conducted to select representative visual stimuli for the new subject, based on Kda-max (maximum probability density), Kda-min (minimum probability density), and random selection. As shown in Table 2, the CLIP metric of the Kda-max method is two points higher than that of the Kda-min method. The results are notably different in terms of high-level metrics, indicating that selecting appropriate visual stimuli can facilitate new subject adaptation. In practical application scenarios, the distribution of new



Table 3: Ablation of different supervision methods in few-shot brain decoding task. The models are evaluated on subject 2.

| Supervision method                     | Low-Level   |             |              |              | High-Level   |              |             |             |
|--|-------------|-------------|--------------|--------------|--------------|--------------|-------------|-------------|
|  | PixCorr↑    | SSIM↑       | Alex(2)↑     | Alex(5)↑     | Incep↑       | CLIP↑        | Eff↓        | SwAV↓       |
| baseline & 1-shot                      | .042        | .217        | 64.2%        | 70.0%        | 62.1%        | 66.4%        | .930        | .600        |
| +cross-subject $\mathcal{L}_{MSE}$     | .088        | <b>.278</b> | 73.5%        | 80.9%        | 71.6%        | 74.9%        | .867        | .545        |
| +cross-subject $\mathcal{L}_{amp}$     | .091        | .275        | 73.9%        | 81.3%        | 71.6%        | 75.6%        | .865        | .541        |
| +cross-subject $\mathcal{L}_{Fourier}$ | <b>.091</b> | .275        | <b>74.1%</b> | <b>81.8%</b> | <b>72.1%</b> | <b>75.6%</b> | <b>.865</b> | <b>.541</b> |
| baseline & 2-shot                      | .052        | .248        | 70.0%        | 77.8%        | 68.2%        | 72.4%        | .900        | .577        |
| +cross-subject $\mathcal{L}_{MSE}$     | .105        | .271        | 76.1%        | 83.4%        | 74.8%        | 77.8%        | .840        | .520        |
| +cross-subject $\mathcal{L}_{amp}$     | <b>.111</b> | .275        | 77.7%        | 86.3%        | 76.0%        | 79.8%        | .833        | .510        |
| +cross-subject $\mathcal{L}_{Fourier}$ | .110        | <b>.275</b> | <b>77.8%</b> | <b>86.6%</b> | <b>78.2%</b> | <b>80.0%</b> | <b>.821</b> | <b>.504</b> |

subjects is often unknown, and the selection of visual stimuli is typically based on random sampling. Consequently, their results fall between Kda-max and Kda-min.

#### 4.4 Ablation study

**Ablation on supervision method.** The key to achieving few-shot brain decoding lies in the Fourier-based cross-subject supervision method equipped with HRF adapter, where effective utilization of prior knowledge from other individuals can enhance accuracy in small sample scenarios. In Table 3, methods with and without cross-subject supervision (baseline) are compared. Additionally, a detailed comparison is conducted between direct supervision of the raw fMRI signal ( $\mathcal{L}_{MSE}$ ), spectral-domain amplitude supervision ( $\mathcal{L}_{amp}$ ), and spectral-domain amplitude and phase supervision ( $\mathcal{L}_{Fourier}$ ). The experiments provide conclusive evidence of the Fourier-based cross-individual supervision method’s effectiveness. Please refer to Appendix A.4 for the ablation study on the HRF adapter architecture.

### 5 Limitations

Above experiments and discussions show several limitations of few-shot brain decoding from fMRI signals. Firstly, due to the difficulty of acquiring high-quality fMRI-image pairs, MindShot is pretrained only on three individuals to gain prior knowledge. The proposed framework needs to be pretrained on a more diverse and larger dataset to obtain more comprehensive prior knowledge. Moreover, visual stimulus selection per category in the few-shot scenario remains difficult. Although this problem is discussed in Section 4.3, where modeling the probability distribution proves effective for selecting reasonable stimuli. However, in practice, due to the scarcity of individual data, it is not possible to select the globally optimal visual stimuli by modeling the statistical distribution of new individuals. Additionally, limited by the fMRI signals that are serialized as 1D vectors in NSD, the fMRI signals lack temporal and spatial information, restricting the model’s ability to capture and decode more complex brain activity information. Lastly, a brain encoder  $\mathcal{E}_{brain}$  is used to align with the high-level CLIP image semantic space, but the image generation process lacked guidance from low-level information (e.g., depth and color), resulting in a lack of detail in reconstructed images.

### 6 Conclusions

In this paper, MindShot, a novel Fourier-based cross-subject brain decoding framework is proposed to achieve few-shot brain decoding. By innovatively addressing the challenges of overfitting, and lack of useful biological guidance, the proposed HRF adapter with Fourier-based cross-subject supervision method is proved to be effective on the NSD dataset and outperforms the per-subject-per-model paradigm. These results not only demonstrate the feasibility of few-shot brain decoding but also provide the possibility for the learning of large models under the condition of reducing data dependence.

## References

- [1] U. Güçlü, M. A. Van Gerven, Deep neural networks reveal a gradient in the complexity of neural representations across the ventral stream, *Journal of Neuroscience* 35 (27) (2015) 10005–10014.
- [2] H. Wen, J. Shi, Y. Zhang, K.-H. Lu, J. Cao, Z. Liu, Neural encoding and decoding with deep learning for dynamic natural vision, *Cerebral cortex* 28 (12) (2018) 4136–4160.
- [3] T. C. Kietzmann, C. J. Spoerer, L. K. Sörensen, R. M. Cichy, O. Hauk, N. Kriegeskorte, Recurrence is required to capture the representational dynamics of the human visual system, *Proceedings of the National Academy of Sciences* 116 (43) (2019) 21854–21863.
- [4] T. Horikawa, Y. Kamitani, Generic decoding of seen and imagined objects using hierarchical visual features, *Nature communications* 8 (1) (2017) 15037.
- [5] C. Qian, X. Sun, Y. Wang, X. Zheng, Y. Wang, G. Pan, Binless kernel machine: Modeling spike train transformation for cognitive neural prostheses, *Neural Computation* 32 (10) (2020) 1863–1900.
- [6] I. Goodfellow, J. Pouget-Abadie, M. Mirza, B. Xu, D. Warde-Farley, S. Ozair, A. Courville, Y. Bengio, Generative adversarial networks, *Communications of the ACM* 63 (11) (2020) 139–144.
- [7] Z. Gu, K. Jamison, A. Kuceyeski, M. Sabuncu, Decoding natural image stimuli from fmri data with a surface-based convolutional network, *arXiv preprint arXiv:2212.02409* (2022).
- [8] F. Ozcelik, B. Choksi, M. Mozafari, L. Reddy, R. VanRullen, Reconstruction of perceived images from fmri patterns and semantic brain exploration using instance-conditioned gans, in: *2022 International Joint Conference on Neural Networks (IJCNN)*, IEEE, 2022, pp. 1–8.
- [9] K. Seeliger, U. Güçlü, L. Ambrogioni, Y. Güçlütürk, M. A. Van Gerven, Generative adversarial networks for reconstructing natural images from brain activity, *NeuroImage* 181 (2018) 775–785.
- [10] J. Ho, A. Jain, P. Abbeel, Denoising diffusion probabilistic models, *Advances in neural information processing systems* 33 (2020) 6840–6851.
- [11] Y. Takagi, S. Nishimoto, High-resolution image reconstruction with latent diffusion models from human brain activity, in: *Proceedings of the IEEE/CVF Conference on Computer Vision and Pattern Recognition*, 2023, pp. 14453–14463.
- [12] P. Scotti, A. Banerjee, J. Goode, S. Shabalin, A. Nguyen, A. Dempster, N. Verlinde, E. Yundler, D. Weisberg, K. Norman, et al., Reconstructing the mind’s eye: fmri-to-image with contrastive learning and diffusion priors, *Advances in Neural Information Processing Systems* 36 (2024).
- [13] Y. Lu, C. Du, Q. Zhou, D. Wang, H. He, Minddiffuser: Controlled image reconstruction from human brain activity with semantic and structural diffusion, in: *Proceedings of the 31st ACM International Conference on Multimedia*, 2023, pp. 5899–5908.
- [14] F. Ozcelik, R. VanRullen, Brain-diffuser: Natural scene reconstruction from fmri signals using generative latent diffusion. *arxiv* 2023, *arXiv preprint arXiv:2303.05334*.
- [15] Z. Chen, J. Qing, J. H. Zhou, Cinematic mindscapes: High-quality video reconstruction from brain activity, *Advances in Neural Information Processing Systems* 36 (2024).
- [16] Z. Chen, J. Qing, T. Xiang, W. L. Yue, J. H. Zhou, Seeing beyond the brain: Conditional diffusion model with sparse masked modeling for vision decoding, in: *Proceedings of the IEEE/CVF Conference on Computer Vision and Pattern Recognition*, 2023, pp. 22710–22720.
- [17] M. A. Lindquist, J. M. Loh, L. Y. Atlas, T. D. Wager, Modeling the hemodynamic response function in fmri: efficiency, bias and mis-modeling, *Neuroimage* 45 (1) (2009) S187–S198.
- [18] H. J. Nussbaumer, H. J. Nussbaumer, *The fast Fourier transform*, Springer, 1982.
- [19] E. J. Allen, G. St-Yves, Y. Wu, J. L. Breedlove, J. S. Prince, L. T. Dowdle, M. Nau, B. Caron, F. Pestilli, I. Charest, et al., A massive 7t fmri dataset to bridge cognitive neuroscience and artificial intelligence, *Nature neuroscience* 25 (1) (2022) 116–126.
- [20] G. Shen, T. Horikawa, K. Majima, Y. Kamitani, Deep image reconstruction from human brain activity, *PLoS computational biology* 15 (1) (2019) e1006633.

- [21] T. Dado, Y. Güçlütürk, L. Ambrogioni, G. Ras, S. Bosch, M. van Gerven, U. Güçlü, Hyperrealistic neural decoding for reconstructing faces from fmri activations via the gan latent space, *Scientific reports* 12 (1) (2022) 141.
- [22] R. VanRullen, L. Reddy, Reconstructing faces from fmri patterns using deep generative neural networks, *Communications biology* 2 (1) (2019) 193.
- [23] C. Du, C. Du, L. Huang, H. Wang, H. He, Structured neural decoding with multitask transfer learning of deep neural network representations, *IEEE Transactions on Neural Networks and Learning Systems* 33 (2) (2020) 600–614.
- [24] R. D. Hjelm, A. Fedorov, S. Lavoie-Marchildon, K. Grewal, P. Bachman, A. Trischler, Y. Bengio, Learning deep representations by mutual information estimation and maximization, *arXiv preprint arXiv:1808.06670* (2018).
- [25] A. Radford, J. W. Kim, C. Hallacy, A. Ramesh, G. Goh, S. Agarwal, G. Sastry, A. Askell, P. Mishkin, J. Clark, et al., Learning transferable visual models from natural language supervision, in: *International conference on machine learning*, PMLR, 2021, pp. 8748–8763.
- [26] R. Rombach, A. Blattmann, D. Lorenz, P. Esser, B. Ommer, High-resolution image synthesis with latent diffusion models, in: *Proceedings of the IEEE/CVF conference on computer vision and pattern recognition*, 2022, pp. 10684–10695.
- [27] Y. Takagi, S. Nishimoto, Improving visual image reconstruction from human brain activity using latent diffusion models via multiple decoded inputs, *arXiv preprint arXiv:2306.11536* (2023).
- [28] W. Xia, R. de Charette, C. Oztireli, J.-H. Xue, Dream: Visual decoding from reversing human visual system, in: *Proceedings of the IEEE/CVF Winter Conference on Applications of Computer Vision*, 2024, pp. 8226–8235.
- [29] S. Wang, S. Liu, Z. Tan, X. Wang, Mindbridge: A cross-subject brain decoding framework, *arXiv preprint arXiv:2404.07850* (2024).
- [30] P. Dhariwal, A. Nichol, Diffusion models beat gans on image synthesis, *Advances in neural information processing systems* 34 (2021) 8780–8794.
- [31] R. Gal, Y. Alaluf, Y. Atzmon, O. Patashnik, A. H. Bermano, G. Chechik, D. Cohen-Or, An image is worth one word: Personalizing text-to-image generation using textual inversion, *arXiv preprint arXiv:2208.01618* (2022).
- [32] N. Ruiz, Y. Li, V. Jampani, Y. Pritch, M. Rubinstein, K. Aberman, Dreambooth: Fine tuning text-to-image diffusion models for subject-driven generation, in: *Proceedings of the IEEE/CVF Conference on Computer Vision and Pattern Recognition*, 2023, pp. 22500–22510.
- [33] T. Brooks, A. Holynski, A. A. Efros, Instructpix2pix: Learning to follow image editing instructions, in: *Proceedings of the IEEE/CVF Conference on Computer Vision and Pattern Recognition*, 2023, pp. 18392–18402.
- [34] A. Blattmann, T. Dockhorn, S. Kulal, D. Mendelevitch, M. Kilian, D. Lorenz, Y. Levi, Z. English, V. Voleti, A. Letts, et al., Stable video diffusion: Scaling latent video diffusion models to large datasets, *arXiv preprint arXiv:2311.15127* (2023).
- [35] X. Yang, D. Zhou, J. Feng, X. Wang, Diffusion probabilistic model made slim, in: *Proceedings of the IEEE/CVF Conference on Computer Vision and Pattern Recognition*, 2023, pp. 22552–22562.
- [36] Z. Wang, Y. Jiang, H. Zheng, P. Wang, P. He, Z. Wang, W. Chen, M. Zhou, et al., Patch diffusion: Faster and more data-efficient training of diffusion models, *Advances in Neural Information Processing Systems* 36 (2024).
- [37] C. Schuhmann, R. Beaumont, R. Vencu, C. Gordon, R. Wightman, M. Cherti, T. Coombes, A. Katta, C. Mullis, M. Wortsman, et al., Laion-5b: An open large-scale dataset for training next generation image-text models, *Advances in Neural Information Processing Systems* 35 (2022) 25278–25294.
- [38] L. Zhang, A. Rao, M. Agrawala, Adding conditional control to text-to-image diffusion models, in: *Proceedings of the IEEE/CVF International Conference on Computer Vision*, 2023, pp. 3836–3847.

- [39] C. Mou, X. Wang, L. Xie, Y. Wu, J. Zhang, Z. Qi, Y. Shan, T2i-adapter: Learning adapters to dig out more controllable ability for text-to-image diffusion models, in: Proceedings of the AAAI Conference on Artificial Intelligence, Vol. 38, 2024, pp. 4296–4304.
- [40] X. Xu, Z. Wang, G. Zhang, K. Wang, H. Shi, Versatile diffusion: Text, images and variations all in one diffusion model, in: Proceedings of the IEEE/CVF International Conference on Computer Vision, 2023, pp. 7754–7765.
- [41] K. He, X. Chen, S. Xie, Y. Li, P. Dollár, R. Girshick, Masked autoencoders are scalable vision learners, in: Proceedings of the IEEE/CVF conference on computer vision and pattern recognition, 2022, pp. 16000–16009.
- [42] A. Oppenheim, J. Lim, G. Kopec, S. Pohlig, Phase in speech and pictures, in: ICASSP’79. IEEE International Conference on Acoustics, Speech, and Signal Processing, Vol. 4, IEEE, 1979, pp. 632–637.
- [43] A. V. Oppenheim, J. S. Lim, The importance of phase in signals, Proceedings of the IEEE 69 (5) (1981) 529–541.
- [44] L. N. Piotrowski, F. W. Campbell, A demonstration of the visual importance and flexibility of spatial-frequency amplitude and phase, Perception 11 (3) (1982) 337–346.
- [45] B. C. Hansen, R. F. Hess, Structural sparseness and spatial phase alignment in natural scenes, JOSA A 24 (7) (2007) 1873–1885.
- [46] Q. Xu, R. Zhang, Y. Zhang, Y. Wang, Q. Tian, A fourier-based framework for domain generalization, in: Proceedings of the IEEE/CVF conference on computer vision and pattern recognition, 2021, pp. 14383–14392.
- [47] A. Ramesh, P. Dhariwal, A. Nichol, C. Chu, M. Chen, Hierarchical text-conditional image generation with clip latents, arXiv preprint arXiv:2204.06125 1 (2) (2022) 3.
- [48] T.-Y. Lin, M. Maire, S. Belongie, J. Hays, P. Perona, D. Ramanan, P. Dollár, C. L. Zitnick, Microsoft coco: Common objects in context, in: Computer Vision–ECCV 2014: 13th European Conference, Zurich, Switzerland, September 6–12, 2014, Proceedings, Part V 13, Springer, 2014, pp. 740–755.
- [49] F. Ozelik, R. VanRullen, Natural scene reconstruction from fmri signals using generative latent diffusion, Scientific Reports 13 (1) (2023) 15666.
- [50] Z. Wang, A. C. Bovik, H. R. Sheikh, E. P. Simoncelli, Image quality assessment: from error visibility to structural similarity, IEEE transactions on image processing 13 (4) (2004) 600–612.
- [51] A. Krizhevsky, I. Sutskever, G. E. Hinton, Imagenet classification with deep convolutional neural networks, Advances in neural information processing systems 25 (2012).
- [52] C. Szegedy, V. Vanhoucke, S. Ioffe, J. Shlens, Z. Wojna, Rethinking the inception architecture for computer vision, in: Proceedings of the IEEE conference on computer vision and pattern recognition, 2016, pp. 2818–2826.
- [53] M. Tan, Q. Le, Efficientnet: Rethinking model scaling for convolutional neural networks, in: International conference on machine learning, PMLR, 2019, pp. 6105–6114.
- [54] M. Caron, I. Misra, J. Mairal, P. Goyal, P. Bojanowski, A. Joulin, Unsupervised learning of visual features by contrasting cluster assignments, Advances in neural information processing systems 33 (2020) 9912–9924.
- [55] L. Van der Maaten, G. Hinton, Visualizing data using t-sne., Journal of machine learning research 9 (11) (2008).
- [56] W. Zhao, L. Bai, Y. Rao, J. Zhou, J. Lu, Unipc: A unified predictor-corrector framework for fast sampling of diffusion models, Advances in Neural Information Processing Systems 36 (2024).
- [57] L. N. Smith, Cyclical learning rates for training neural networks, in: 2017 IEEE winter conference on applications of computer vision (WACV), IEEE, 2017, pp. 464–472.

## A Appendix

### A.1 Implementation details

In this paper, the versatile diffusion model is employed for image reconstruction. During the diffusion process, the UniPCMultistep scheduler [56] is utilized to execute 20 steps, with a guidance scale of 3.5. During the new-subject adaptation phase, the total loss is balanced by setting the weights of  $\mathcal{L}_{SoftCLIP}$ ,  $\mathcal{L}_{prior}$ ,  $\mathcal{L}_{amp}$ ,  $\mathcal{L}_{pha}$  to 1, 30, 2, and 2 respectively. MindShot is trained for 240 epochs, with a batch size of 64 during the prior knowledge pretrain phase and 32 during the new-subject adaptation phase. The cyclical learning rate approach [57] is adopted for learning rate scheduling across all training phases, with the maximum learning rate set to  $3e-4$ . Our experiments are conducted on a single NVIDIA 80GB A100 GPU. The pre-training phase required approximately 17 hours and 48GB of memory, while the new subject few-shot adaptation phase only required one hour and 27GB of memory.

### A.2 Few-shot brain decoding task

In the few-shot brain decoding task, the visual stimuli for new subjects are categorized into 80 classes, with the images within each class sorted according to the file naming convention of the NSD dataset. Subsequently, a few initial images are selected from each class to construct a few-shot subset. This approach not only ensures same training data for ablation experiments but also simulates real-world application scenarios.

### A.3 Architecture of MindShot

The AdaptiveMaxPool1D is employed to standardize the scales of different individuals' fMRI signals, ensuring consistency by resizing them to a length of 9600. This step is integrated into the data preprocessing pipeline of the dataloader. In MindShot, brain activity encoding is divided into a subject-specific HRF adapter and a shared brain encoder. The HRF adapter is designed as a 1-layer residual Multilayer Perceptron (MLP) structure, with both the input and output of the linear layer being 9600. The brain encoder is a MLP structure, consisting of a backbone and two projectors. The backbone includes one linear layer with an output size of 4096, followed by a 4-layer residual MLP, and then utilizes a linear layer to map features to a size of  $257 \times 768$ . The projectors comprise an image projector and a prior network [12]. The image projector is designed as a 3-layer MLP with a hidden size of 2048, and the final layer output is  $257 \times 768$ . Visual stimuli are encoded using CLIP ViT-L/14, with a semantic embedding size of  $257 \times 768$ . The HRF adapter has 92M parameters, while the brain encoder has 978M parameters.

### A.4 Ablation on HRF adapter architecture

The structural design results of the HRF adapter are presented in Table 4, which compares 3-layer, 2-layer, and 1-layer architectures. In the 1-shot scenario, it is observed that the 2-layer structure slightly outperforms the 1-layer structure in terms of high-level metrics. However, in the 2-shot scenario, the 1-layer structure performs better. Considering the reduction in training cost and storage overhead, the structure with a smaller number of parameters is chosen. Moreover, it is discovered that the residual structure performed better among the 1-layer architectures, showing that leveraging the hemodynamic response function to model individual differences and applying it to the design of adapter can effectively improve the performance of the model.

### A.5 Visualization of Fourier supervision method

As shown in Figure 5, the visualization of fMRI signals before and after Fourier supervision is presented. By employing a cross-subject approach and a learnable HRF adapter, the amplitude and phase of fMRI signals in the spectral domain are adjusted, thereby reducing the variability between different subjects.

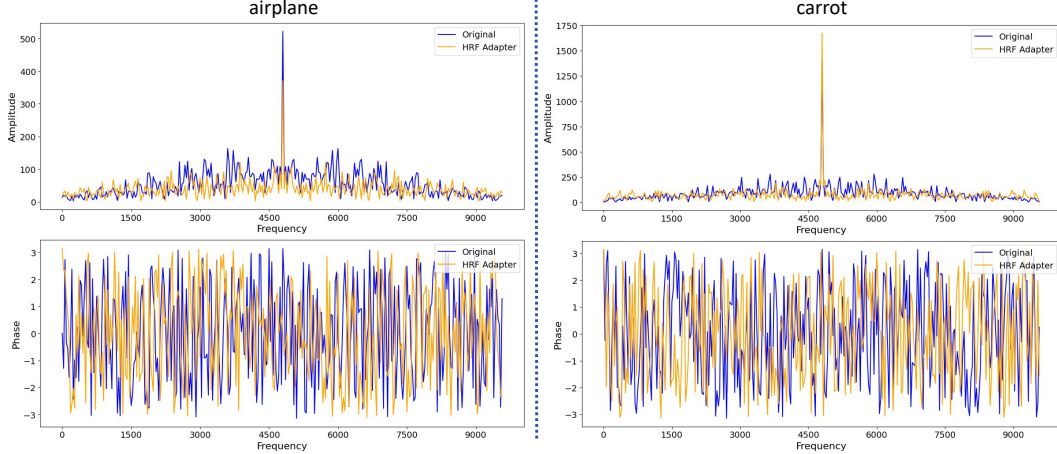


Figure 5: Examples of Fourier-based cross-subject supervision. We present fMRI signals related to semantic categories like airplane and carrot from subject 5. The blue line represents the original fMRI signal, while the orange line represents the fMRI signal after correction with the HRF adapter.

Table 4: Ablation of HRF adapter architecture in few-shot brain decoding task. The models are evaluated on subject 2. FC represents the fully connected layer.

| Architecture            | Low-Level          |                 |                    |                    | High-Level       |                 |                  |                   |
|-------------------------|--------------------|-----------------|--------------------|--------------------|------------------|-----------------|------------------|-------------------|
|                         | PixCorr $\uparrow$ | SSIM $\uparrow$ | Alex(2) $\uparrow$ | Alex(5) $\uparrow$ | Incep $\uparrow$ | CLIP $\uparrow$ | Eff $\downarrow$ | SwAV $\downarrow$ |
| 3-layer FC & 1-shot     | .088               | .273            | 71.7%              | 80.6%              | 70.7%            | 74.5%           | .880             | .552              |
| 2-layer FC & 1-shot     | .085               | .272            | 73.4%              | <b>82.2%</b>       | <b>72.4%</b>     | <b>75.9%</b>    | <b>.872</b>      | .541              |
| 1-layer FC w/o residual | .084               | .274            | 73.3%              | 81.6%              | 71.6%            | 76.1%           | .868             | .546              |
| 1-layer FC & 1-shot     | <b>.091</b>        | <b>.275</b>     | <b>74.1%</b>       | 81.8%              | 72.1%            | 75.6%           | .865             | <b>.541</b>       |
| 3-layer FC & 2-shot     | .095               | .265            | 76.1%              | 85.1%              | 76.2%            | 80.3%           | .840             | .515              |
| 2-layer FC & 2-shot     | .111               | .274            | 77.1%              | 85.6%              | 77.5%            | 80.2%           | .838             | .516              |
| 1-layer FC w/o residual | .106               | .275            | 77.4%              | 86.3%              | 76.9%            | <b>80.3%</b>    | .834             | .508              |
| 1-layer FC & 2-shot     | <b>.110</b>        | <b>.275</b>     | <b>77.8%</b>       | <b>86.6%</b>       | <b>78.2%</b>     | 80.0%           | <b>.821</b>      | <b>.504</b>       |

## A.6 More results for few-shot brain decoding

Here, additional few-shot brain decoding results for subjects 1, 2, 5, and 7 are presented in Table 5, Table 6, Table 7, and Table 8. These results demonstrate that the MindShot method consistently outperforms the per-subject-per-model paradigm in all few-shot scenarios and for all subjects.

## A.7 Ethic and social impact

This paper utilized the publicly available NSD dataset and introduced MindShot, a novel approach that not only achieved few-shot brain decoding but also accelerated the practical application of BCIs in real-world scenarios. As brain decoding technology advances, it raises critical ethical considerations. While this technology offers improved communication methods for individuals with disabilities, its potential for involuntary mind reading necessitates strict ethical frameworks. The scientific community and society need to collaborate in preventing the misuse of brain decoding technology.



Table 5: Results of few-shot brain decoding for subject 1. MindShot (Ours) is pretrained on subject 2,5 and 7.

| Method         | Data   | Low-Level   |             |              |              | High-Level   |              |             |             |
|----------------|--------|-------------|-------------|--------------|--------------|--------------|--------------|-------------|-------------|
|                |        | PixCorr↑    | SSIM↑       | Alex(2)↑     | Alex(5)↑     | Incep↑       | CLIP↑        | Eff↓        | SwAV↓       |
| MindEye        | 1-shot | .047        | .225        | 63.8%        | 69.8%        | 61.4%        | 66.8%        | .925        | .596        |
| MindShot(Ours) | 1-shot | <b>.104</b> | <b>.256</b> | <b>74.9%</b> | <b>83.2%</b> | <b>73.9%</b> | <b>77.2%</b> | <b>.852</b> | <b>.532</b> |
| MindEye        | 2-shot | .079        | .233        | 69.1%        | 76.3%        | 68.2%        | 73.0%        | .890        | .570        |
| MindShot(Ours) | 2-shot | <b>.127</b> | <b>.255</b> | <b>77.6%</b> | <b>86.4%</b> | <b>78.4%</b> | <b>81.8%</b> | <b>.817</b> | <b>.500</b> |
| MindEye        | 3-shot | .083        | .252        | 72.2%        | 79.4%        | 70.1%        | 74.5%        | .877        | .552        |
| MindShot(Ours) | 3-shot | <b>.133</b> | <b>.260</b> | <b>80.4%</b> | <b>89.1%</b> | <b>82.0%</b> | <b>83.2%</b> | <b>.789</b> | <b>.484</b> |

Table 6: Results of few-shot brain decoding for subject 2. MindShot (Ours) is pretrained on subject 1,5 and 7.

| Method         | Data   | Low-Level   |             |              |              | High-Level   |              |             |             |
|----------------|--------|-------------|-------------|--------------|--------------|--------------|--------------|-------------|-------------|
|                |        | PixCorr↑    | SSIM↑       | Alex(2)↑     | Alex(5)↑     | Incep↑       | CLIP↑        | Eff↓        | SwAV↓       |
| MindEye        | 1-shot | .042        | .217        | 64.2%        | 70.0%        | 62.1%        | 66.4%        | .930        | .600        |
| MindShot(Ours) | 1-shot | <b>.091</b> | <b>.275</b> | <b>74.1%</b> | <b>81.8%</b> | <b>72.1%</b> | <b>75.6%</b> | <b>.865</b> | <b>.541</b> |
| MindEye        | 2-shot | .052        | .248        | 70.0%        | 77.8%        | 68.2%        | 72.4%        | .900        | .577        |
| MindShot(Ours) | 2-shot | <b>.110</b> | <b>.275</b> | <b>77.8%</b> | <b>86.6%</b> | <b>78.2%</b> | <b>80.0%</b> | <b>.821</b> | <b>.504</b> |
| MindEye        | 3-shot | .067        | .262        | 70.9%        | 78.7%        | 70.4%        | 74.5%        | .883        | .562        |
| MindShot(Ours) | 3-shot | <b>.115</b> | <b>.277</b> | <b>78.8%</b> | <b>87.8%</b> | <b>81.0%</b> | <b>82.7%</b> | <b>.804</b> | <b>.486</b> |

Table 7: Results of few-shot brain decoding for subject 5. MindShot (Ours) is pretrained on subject 1,2 and 7.

| Method         | Data   | Low-Level   |             |              |              | High-Level   |              |             |             |
|----------------|--------|-------------|-------------|--------------|--------------|--------------|--------------|-------------|-------------|
|                |        | PixCorr↑    | SSIM↑       | Alex(2)↑     | Alex(5)↑     | Incep↑       | CLIP↑        | Eff↓        | SwAV↓       |
| MindEye        | 1-shot | .054        | .221        | 62.0%        | 70.6%        | 64.1%        | 69.5%        | .916        | .590        |
| MindShot(Ours) | 1-shot | <b>.096</b> | <b>.253</b> | <b>73.6%</b> | <b>83.4%</b> | <b>77.0%</b> | <b>80.7%</b> | <b>.825</b> | <b>.516</b> |
| MindEye        | 2-shot | .077        | .233        | 68.0%        | 77.7%        | 71.1%        | 74.9%        | .882        | .563        |
| MindShot(Ours) | 2-shot | <b>.115</b> | <b>.255</b> | <b>75.9%</b> | <b>86.8%</b> | <b>82.3%</b> | <b>84.2%</b> | <b>.791</b> | <b>.484</b> |
| MindEye        | 3-shot | .100        | .245        | 72.0%        | 80.9%        | 74.1%        | 78.2%        | .857        | .534        |
| MindShot(Ours) | 3-shot | <b>.120</b> | <b>.265</b> | <b>78.6%</b> | <b>88.8%</b> | <b>83.9%</b> | <b>86.4%</b> | <b>.767</b> | <b>.466</b> |

Table 8: Results of few-shot brain decoding for subject 7. MindShot (Ours) is pretrained on subject 1,2 and 5.

| Method         | Data   | Low-Level   |             |              |              | High-Level   |              |             |             |
|----------------|--------|-------------|-------------|--------------|--------------|--------------|--------------|-------------|-------------|
|                |        | PixCorr↑    | SSIM↑       | Alex(2)↑     | Alex(5)↑     | Incep↑       | CLIP↑        | Eff↓        | SwAV↓       |
| MindEye        | 1-shot | .044        | .190        | 59.1%        | 65.3%        | 58.5%        | 62.9%        | .938        | .616        |
| MindShot(Ours) | 1-shot | <b>.098</b> | <b>.257</b> | <b>72.5%</b> | <b>79.0%</b> | <b>71.8%</b> | <b>74.8%</b> | <b>.869</b> | <b>.544</b> |
| MindEye        | 2-shot | .068        | .234        | 67.0%        | 71.5%        | 62.5%        | 68.0%        | .913        | .587        |
| MindShot(Ours) | 2-shot | <b>.116</b> | <b>.264</b> | <b>76.2%</b> | <b>83.6%</b> | <b>76.3%</b> | <b>80.1%</b> | <b>.835</b> | <b>.508</b> |
| MindEye        | 3-shot | .067        | .236        | 69.3%        | 76.7%        | 66.3%        | 72.9%        | .898        | .572        |
| MindShot(Ours) | 3-shot | <b>.118</b> | <b>.264</b> | <b>77.4%</b> | <b>85.8%</b> | <b>79.4%</b> | <b>81.5%</b> | <b>.815</b> | <b>.491</b> |